To appear in *Vehicle System Dynamics*
Vol. 00, No. 00, Month 20XX, 1–15

A new formulation of the understeer coefficient to relate yaw torque and vehicle handling.

F. Bucchi* and F. Frendo

[a] *Università di Pisa, Largo Lucio Lazzarino, 56122, Pisa, Italy*

(*Received 00 Month 20XX; accepted 00 Month 20XX*)

The handling behavior of vehicles is an important property for its relation to performance and safety issues. In 1970s Pacejka did the groundwork for an objective analysis introducing the handling diagram and the understeer coefficient, based on a simplified single-track model. In more recent years the understeer concept is still mentioned but the handling is actively managed by Direct Yaw Control (DYC).

In this paper an accurate analysis of the vehicle handling is carried out, considering also the effect of drive forces. This analysis brought to a new formulation of the understeer coefficient, which is almost equivalent to the classical one, but it can be obtained by simple measures on real vehicles. In addition, it relates the vehicle yaw torque to the understeer coefficient, filling up the gap between the classical handling approach and the DYC.

A multibody model of a Formula SAE car was used to perform quasi-steady state simulations in order to verify the effectiveness of the new formulation. Some vehicle set-ups and wheel drive arrangements were simulated and the results are discussed. In particular, the handling behaviors of the rear wheel drive (RWD) and the front wheel drive (FWD) architectures were compared, finding an apparently surprisingly result: for the analyzed vehicle the FWD is less understeering than for RWD.

The relation between the yaw torque and the understeer coefficient allowed to understand this behavior and seems to be an useful tool in independent wheel drive control.

Keywords: vehicle dynamics; handling diagram; Formula SAE; understeer; wheel drive; yaw control.

1. Introduction

The turning behavior of vehicles is a very important characteristic due to its strict correlation with the vehicle safety and performance. The steady-state turning analysis was introduced by Pacejka [1] in 1973, who defined the handling diagram and the over/neutral/understeer (understeer coefficient in the following) concepts, which are believed as fundamental cornerstones in vehicle dynamics. The handling diagram depicts the cornering behavior of the vehicle as a function of the sole lateral acceleration in the whole operating range (from no lateral acceleration to the adherence limit). The understeer coefficient gives a measure of the wheel steering change as a function of the lateral acceleration. This approach, which was developed on the basis of the single-track (or bicycle) model, is very useful in most cases, even if it is confined to very small slip and steering angles.

Corresponding author. Email: francesco.bucchi@for.unipi.it

More recently, a more general approach was proposed by Frendo et al. [2–4], who extended the concept of understeer, showing its dependence on both the lateral acceleration and another parameter, e.g. the steering wheel angle, the vehicle speed or the turning radius [2, 3]. In particular, they also discussed the influence of drive forces on the yaw torque at steady state, as in the case of locked differential [4].

Even if in the technical literature there are many papers dealing with direct yaw control (DYC), very few papers, beyond the ones cited above, deal with a through analysis of the steady state turning behavior of a vehicle from a physical point of view. On the contrary, many papers deal with non steady-state yaw control. The DYC consists in imposing separately traction or braking forces to the different wheels to stabilize the vehicle behavior. In [5], the β-method is introduced as a way of assessing the steering effect on the yaw behavior of a vehicle as a function of the center of gravity side-slip β. In particular, it was found that as the side-slip rises the vehicle becomes unstable and the influence of steering on the yaw torque reduces. For this reason, Furukawa et al. [6] proposed a method to control the side-slip angle based on 4 wheel steering (4WS) and DYC. 4WS is very accurate before the tire lateral force saturation, whereas DYC is effective also for high lateral accelerations. The β-method was also used by Bosch [7] in the electronic stability program (ESP), which foresees the use of traction and braking force to stabilize the vehicle.

Recently the capability of electric drive to control independently the torque at each wheel with low time-lag, both in traction and braking, allowed to consider more accurate strategies for DYC. Shino [8] proposed a DYC algorithm in order to maintain the vehicle side slip constant and equal to 0 during dynamic maneuvers and verified it with numerical simulations. Osborn et al. [9] determined, on the basis of Dugoff tire model [10], the sensitivity of the vehicle yaw to the distribution of individual drive forces in an AWD. The Dugoff model was also used by Piyabongkarn et al. [11] which concluded, considering the yaw rate derivative in very a simplified model (without load transfers), that the rear drive wheel induces oversteer. Considering steady state maneuvers, Liang et al. [12] proposed a yaw moment control which maximizes the axle yaw moment due to longitudinal forces without modifying the total traction (or braking) force. This method does not affect the perception of driver in terms of longitudinal acceleration but, as stated in [13], due to the scrub radius, the traction force can generate change in the steering wheel torque.

In terms of vehicle performance, several efforts have been done in order to use the longitudinal forces to increase the lateral acceleration limit by simultaneously exploiting the four wheels maximum adherence, optimizing the lateral and longitudinal forces [14–16].

In almost all the cited papers the focus was on the vehicle yaw control and strongly simplified models were often used for both tire behavior and vehicle dynamics. In this paper, a new approach is proposed to relate the useful steady state analysis (handling diagram and understeer coefficient) to the yaw torque. In particular an alternative expression of the understeer coefficient is obtained starting from quasi-steady state maneuvers which can be easily performed on actual vehicles. The new understeer coefficient formulation is based on the knowledge of the trajectory curvature time derivative or of the yaw torque deriving from all the tire forces.

Some simulations were carried out in order to validate such new expression of the understeer coefficient. A 15-dof multibody model of a Formula SAE car [17] was used to perform the simulations, which consisted in constant longitudinal and constant steering rate maneuvers. The PAC2002 [18] model which considers the combined tire slips was used to simulate the tire forces. Several vehicle configurations were chosen to highlight the influence of car set-up on the yaw torque and on the understeer coefficient, including

the effect of rear or front drive.

Some new concepts are also derived, which may be considered in the yaw control strategies.

2. Vehicle dynamic equilibrium

Nowadays the dynamic analyses of vehicles are performed with complex models which take into account many details of the vehicle dynamics, even if many basic concepts can be understood with simplified model. For this reason, before performing the multibody simulations described in Section 5, the double-track model shown in Fig. 1 is considered. This model is needed to write the dynamic equations of the vehicle, which are used to draw the handling parameters as the understeer coefficient in both the classical and the new formulation.

The scheme refers to a left turn and an all-wheel drive vehicle. This model is composed of one rigid body (no suspension kinematics is considered) moving on the plane and having 3 dof. The origin of the reference frame is assumed in correspondence of the projection of the vehicle center of mass G on the horizontal plane. The vehicle wheelbase is l, the front track is t_1 and the rear track is t_2. The distance along the x-axis between the front [rear] axle and G is called a_1 [a_2]. The wheels steer angles are δ_{ij}, where the first subscript i identifies the axle ($i = 1$ is front, $i = 2$ is rear) and the second subscript j identifies the side ($j = 1$ is left, $j = 2$ is right). The rear wheels are not assumed to steer.

Figure 1 shows also the forces and the moments acting on each wheel. In particular the longitudinal tire forces are called X_{ij}, the lateral tire forces are called Y_{ij}. In this model, the forces are supposed to be applied in the center of the tire contact patch and the self-aligning moments M_{ij} are taken into account to consider the real point of application of the lateral forces. Since the vehicle motion is assumed plane and the yaw rate r is not

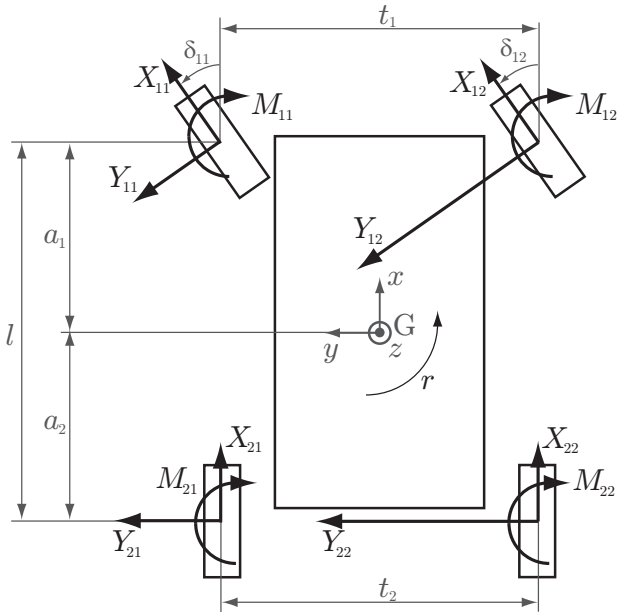

Figure 1. Double-track vehicle model - Dimensions and forces.

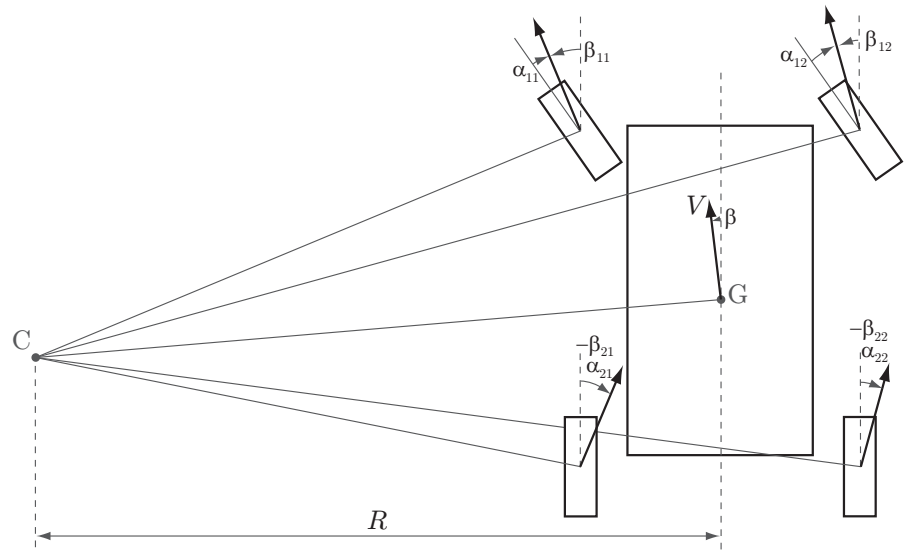

Figure 2. Double-track vehicle model - Kinematics and slip angles.

0, it is possible to define the instantaneous center of velocity C. The velocity $\mathbf{V}$ of G is

$$\mathbf{V} = r\hat{\mathbf{k}} \times CG = u\hat{\mathbf{i}} + v\hat{\mathbf{j}} \tag{1}$$

where $\hat{\mathbf{i}}$, $\hat{\mathbf{j}}$, $\hat{\mathbf{k}}$ are the unit vectors along x, y and z axes, and u and v are the longitudinal and lateral velocity respectively. The side-slip angle β, computed in G, is

$$\beta = \arctan\left(\frac{v}{u}\right) \tag{2}$$

and similarly the side-slip angle β_{ij} can be computed at each wheel considering the longitudinal and lateral velocity at each point (Fig. 2). The slip angles α_{ij} are finally computed as follows

$$\alpha_{ij} = \delta_{ij} - \beta_{ij}. \tag{3}$$

The trajectory curvature ρ, which is the reciprocal of the turning radius R represented in Fig. 2, can be computed starting from the yaw rate and the longitudinal speed as follows

$$\rho = \frac{r}{u}. \tag{4}$$

The longitudinal, lateral and yaw equilibrium of the vehicle are expressed by

$$m(\dot{u} - \beta\rho u^2) = X = X_{11}\cos\delta_{11} + X_{12}\cos\delta_{12} + X_{21} + X_{22} - Y_{11}\sin\delta_{11} - Y_{12}\sin\delta_{12} \tag{5a}$$

$$m(\dot{\beta}u + \dot{u}\beta + \rho u^2) = Y = Y_{11}\cos\delta_{11} + Y_{12}\cos\delta_{12} + Y_{21} + Y_{22} + X_{11}\sin\delta_{11} + X_{12}\sin\delta_{12} \tag{5b}$$

$$J(\dot{\rho}u + \dot{u}\rho) = N = (Y_{11}\cos\delta_{11} + Y_{12}\cos\delta_{12} + X_{11}\sin\delta_{11} + X_{12}\sin\delta_{12})a_1 - (Y_{21} + Y_{22})a_2 + \\ + (X_{12}\cos\delta_{12} - X_{11}\cos\delta_{11})t_1/2 + (X_{22} - X_{21})t_2/2 + \\ + (Y_{11}\sin\delta_{11} - Y_{12}\sin\delta_{12})t_1/2 - (M_{11} + M_{12} + M_{21} + M_{22}), \tag{5c}$$

where m is the vehicle mass and J is the yaw moment, X, Y and N are the sum of longitudinal forces, lateral forces and yaw moments respectively, evaluated with respect to the vehicle reference frame introduced in Fig. 1. The aerodynamic forces, the tire rolling resistance forces and the road slope are neglected. In addition to the planar equilibrium, also the load transfer and the combined non-linear longitudinal and lateral tire characteristics have to be considered. These expression can be found in [19] and are considered in the multibody analysis. Indeed, Eq. 5 can not be solved analytically but some preliminary general observations can be done.

3. Understeer gradient and yaw torque for constant speed maneuver

3.1. *Understeer gradient*

Starting from the previous Eq. 5 and assuming the lateral acceleration a_y and the steering angle δ_w as state variables, the steady-state map $(\tilde{\beta}, \tilde{\rho})$ can be computed considering steady state conditions ($\dot{u} = \dot{\beta} = \dot{\rho} = 0$). The gradients of $\tilde{\beta}$ and $\tilde{\rho}$ can be defined following [19]

$$\nabla\tilde{\beta} = \left(\frac{\partial\tilde{\beta}}{\partial a_y}, \frac{\partial\tilde{\beta}}{\partial\delta_w}\right) = (\beta_y, \beta_\delta) \tag{6a}$$

$$\nabla\tilde{\rho} = \left(\frac{\partial\tilde{\rho}}{\partial a_y}, \frac{\partial\tilde{\rho}}{\partial\delta_w}\right) = (\rho_y, \rho_\delta)\,. \tag{6b}$$

Considering the curvature gradient $\nabla\tilde{\rho}$, it can be demonstrated [19] that

$$\rho_y = -\frac{1}{l}\frac{\partial(\alpha_1 - \alpha_2)}{\partial a_y} = -\frac{1}{l}\frac{\partial(\delta - l\rho)}{\partial a_y} = -\frac{K}{l} \tag{7a}$$

$$\rho_\delta = \frac{\tau}{l}, \tag{7b}$$

where K is the understeer coefficient as introduced by Pacejka [1] and τ is the gear ratio of the steering system, which, for simplicity, is assumed equal for the internal and the external front wheel (parallel steering)

$$\tau = \frac{\delta_{11}}{\delta_w} = \frac{\delta_{12}}{\delta_w}. \tag{8}$$

3.2. *Yaw torque analysis*

In order to simplify the analysis and to span the whole lateral acceleration range, this analysis deals with quasi-steady state conditions. In particular, constant speed ($\dot{u} = 0$, $u = const.$) and constant steering wheel rate maneuvers ($\ddot{\delta}_w = 0$, $\dot{\delta}_w = const.$) are considered. It is worth noting that this maneuver is representative of many normal driving operations. Indeed, in normal driving, the vehicle speed is imposed by the throttle request and the speed varies on the basis of engine response and vehicle inertia, with a relatively long time constant. On the contrary the steering angle of the front wheels is directly applied by the driver by the steering wheel and its response is faster. Under these conditions, the inertial terms of Eq. 5 are

$$-m\beta\rho u^2 = \tilde{X} \tag{9a}$$

$$m(\dot{\beta}u + \rho u^2) = \tilde{Y} \tag{9b}$$

$$J\dot{\rho}u = \tilde{N}. \tag{9c}$$

It is worth noting that, even if the speed is constant and no aerodynamic or tire rolling resistance forces are considered, the resultant of the longitudinal forces $\tilde{X}$ is not zero due to the effect of the slip angle β.

Considering the yaw moment equation (Eq. 9c), the total curvature derivative $\dot{\rho}$ can be expressed as follows

$$\dot{\rho} = \frac{\mathrm{d}\rho\left(t, a_y(t), \delta(t)\right)}{\mathrm{d}t} = \frac{\partial\rho}{\partial t} + \frac{\partial\rho}{\partial a_y}\frac{\mathrm{d}a_y}{\mathrm{d}t} + \frac{\partial\rho}{\partial\delta_w}\frac{\mathrm{d}\delta_w}{\mathrm{d}t}. \tag{10}$$

In the previous equations, if the steering wheel speed is low, the quasi-steady state condition is verified, then, the partial derivative $\frac{\partial\rho}{\partial t}$ can be neglected and the partial derivative terms defined in Eq. 7a and Eq. 7b can be used to obtain

$$\dot{\rho} \simeq -\frac{K}{l}\dot{a}_y + \frac{\tau}{l}\dot{\delta}_w. \tag{11}$$

The term $\dot{a}_y$ can be obtained starting from the lateral acceleration definition for constant speed maneuvers

$$\dot{a}_y = \frac{\mathrm{d}(\dot{\beta}u + \rho u^2)}{\mathrm{d}t} = \ddot{\beta}u + \dot{\rho}u^2 \simeq \dot{\rho}u^2 \tag{12}$$

where in normal driving conditions it can be reasonably assumed that $\ddot{\beta}u \ll \dot{\rho}u^2$. Substituting Eq. 12 in Eq. 11, a new definition of the understeer coefficient can be obtained

$$K \simeq \frac{1}{u^2}\left(\frac{\tau\dot{\delta}_w}{\dot{\rho}} - l\right), \tag{13}$$

which can be written in an alternative way as a function of the yaw torque $\tilde{N}$

$$K \simeq \frac{1}{u^2}\left(\frac{\tau\dot{\delta}_w J u}{\tilde{N}} - l\right). \tag{14}$$

Equation 13 allows to evaluate the understeer coefficient on the basis of $\dot{\delta}_w$ and $\dot{\rho}$, e.g. by using an encoder on the steering wheel and two accelerometers in two different positions of the vehicle or, alternatively, an encoder and a gyro sensor. It is worth noting that, using Eq. 13, the understeer coefficient can be measured experimentally without requiring an accurate vehicle model or the knowledge of the tire characteristics. In addition, in many cases, the understeer coefficient is computed starting from the values of the slip angles, which can be computed only if the vehicle side-slip angle β is known (Eq. 3). Using Eq. 13 the measure of β, which is difficult to be acquired, is no more necessary.

Equation 14 is very important since it opens-up the possibility to control the vehicle turning behavior actively, since it relates the classical definition of understeer to the yaw torque. Indeed, when a target value $\bar{K}$ of understeer is assumed, by measuring the steering wheel speed $\dot{\bar{\delta}}_w$, the actual understeer coefficient is assessed by Eq. 13, the yaw torque variation ΔN can be controlled proportionally to the understeer coefficient error

$$\Delta N = k_y(\bar{K} - K) \tag{15}$$

where k_y is a parameter to be tuned, which depends on the specific vehicle parameters. The torque control following the logic proposed in Eq. 15 can be used both for vehicle performance and vehicle safety.

4. Drive force effect on the yaw torque

In the classical steady-state analysis, the influence of drive forces on the yaw torque is neglected because the problem is linearized and it is assumed that, even if the steering wheel angle is not zero, the drive forces act longitudinally with respect to the vehicle reference frame defined in Fig. 1. If a locked differential is considered the influence of drive forces arises explicitly [4]. However, even if the differential is open and FWD or AWD vehicles are considered, the drive forces influence also the lateral and yaw dynamics.

Indeed, the longitudinal equilibrium stated in Eq. 9a shows that, if ρ and β are not zero, the drive forces are required to keep the speed constant. In addition, considering the lateral equilibrium Eq. 5b, it is worth noting that, in FWD and AWD, a part of the drive forces contributes to the lateral equilibrium. Finally, considering Eq. 5c, in addition to the usually considered contribution of the tire lateral forces and self-aligning moment T_Y (Eq. 16a), other terms contribute to the yaw equilibrium. In particular, in FWD and AWD the front wheel drive forces produce the yaw moment T_f (Eq. 16b), while in the case of non-open differentials, the yaw torque T_d (Eq. 16c) due to the difference along the x-axis between right and left longitudinal forces has to be considered. In general:

$$T_Y = (Y_{11}\cos\delta_{11} + Y_{12}\cos\delta_{12})a_1 - (Y_{21}+Y_{22})a_2 + (Y_{11}\sin\delta_{11} - Y_{12}\sin\delta_{12})t_1/2 + \\ -(M_{11}+M_{12}+M_{21}+M_{22}) \tag{16a}$$

$$T_f = (X_{11}\sin\delta_{11} + X_{12}\sin\delta_{12})a_1 \tag{16b}$$

$$T_d = (X_{12}\cos\delta_{12} - X_{11}\cos\delta_{11})t_1/2 + (X_{22} - X_{21})t_2/2 \tag{16c}$$

It is worth noting that the sign of T_f is always positive in left turn maneuver. On the contrary, the sign of T_d can not be predicted easily and its effect is discussed deeply in [4]. Similar considerations could be done in right turn. In any case, T_f is concordant with the steering angle and the yaw rate.

These yaw torques, which are produced by the drive forces, are usually neglected in the steady-state analysis but affect the vehicle handling, especially for high steering and lateral acceleration values, as it will be shown.

5. Multibody simulation

In order to perform skid maneuvers and to verify the new formulation of understeer coefficient given in Eq. 13, a multibody model of a Formula SAE car, already developed by the authors in MSC Adams View environment and presented in [17], was used. The effects on the vehicle turning behavior of set-up parameters (i.e. front/rear roll stiffness) and drive architecture were simulated.

5.1. *Model description*

The model has 15 degrees of freedom (dof): 6-dof are related to the sprung mass motion, 4-dof to the wheels rotation, 4-dof to the suspensions motion and 1-dof to the steering wheel rotation. The wheelbase is 1580 mm, the front track is 1210 mm, the rear track is 1110 mm and the vehicle mass, including the driver, is 285 kg. The center of mass inertia tensor is principal and the yaw moment of inertia J is 163 kgm^2.

The steering wheel is connected to the front wheels by a rack-pinion system which guarantees parallel steering in the whole operating range. Both front and rear suspension architecture is double non-parallel A-arm with push rod and tunable anti-roll bar. The tires characteristics, which were supplied by the Formula SAE Tire Test Consortium, are imported as PAC2002 parameters [18] and include the vertical, lateral, drive, self-aligning and combined effects.

The traction and braking torques can be imposed separately to each wheel.

5.2. *Maneuvers and vehicle configurations description*

A constant speed and constant steering wheel rate maneuver was considered. The target speed value was 15 m/s, whereas the steering wheel rate $\dot{\delta}_w$ was kept constant at 2 deg/s in order to perform quasi-steady state maneuvers.

The speed was imposed as a target value u_T and a proportional control was developed in order to act on the total torque T supplied to the drive wheels as follows

$$T = k(u_T - u) \tag{17}$$

where u is the measured speed of the center of mass of the vehicle and k is the torque gain which was set to 7500 Ns.

The torque was computed for each wheel as follows

$$T_{1j} = \nu \frac{T}{2} \tag{18a}$$

$$T_{2j} = (1 - \nu) \frac{T}{2} \tag{18b}$$

where ν is the front to rear traction ratio.

Four vehicle configurations were considered:

- rear wheel drive, medium roll stiffness on both front and rear axles (reference configuration - RWD-m);
- rear wheel drive, high roll stiffness on front axle and low roll stiffness on rear axle (more understeering than reference - RWD-u);
- rear wheel drive, low roll stiffness on front axle and high roll stiffness on rear axle (more oversteering than reference - RWD-o);
- front wheel drive, medium roll stiffness on both front and rear axles (FWD-m).

Each simulation started with the vehicle in straight line at constant speed ($u = 15$ m/s, $\delta_w = 0$) and then the steering wheel angle started increasing. For each simulation it was verified that the speed was kept almost constant and equal to the reference value u_T (with variations below 1%), as proved by Fig. 3. Each simulation was interrupted when the lateral acceleration of the sprung mass started decreasing, meaning that the adherence limit was reached.

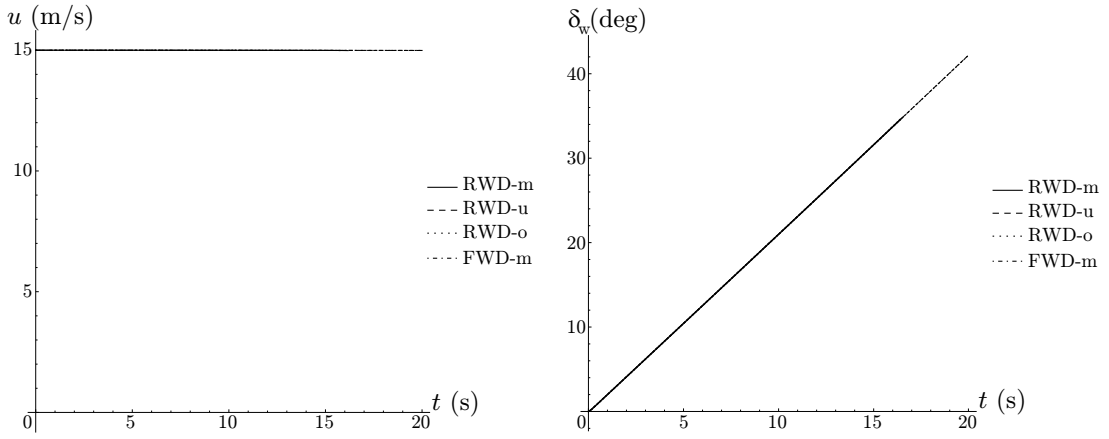

(a) a) (b) b)

Figure 3. Actual vehicle speed (a) and steering wheel (b) time history.

6. Results

The lateral acceleration time history is shown in Fig. 4 for all the simulations. Even if the simulations were performed with the same vehicle and only set-up and drive architecture were changed, the handling behavior is considerably different between each configuration. In particular, considering as reference the RWD-m set-up, the FWD-m and RWD-o

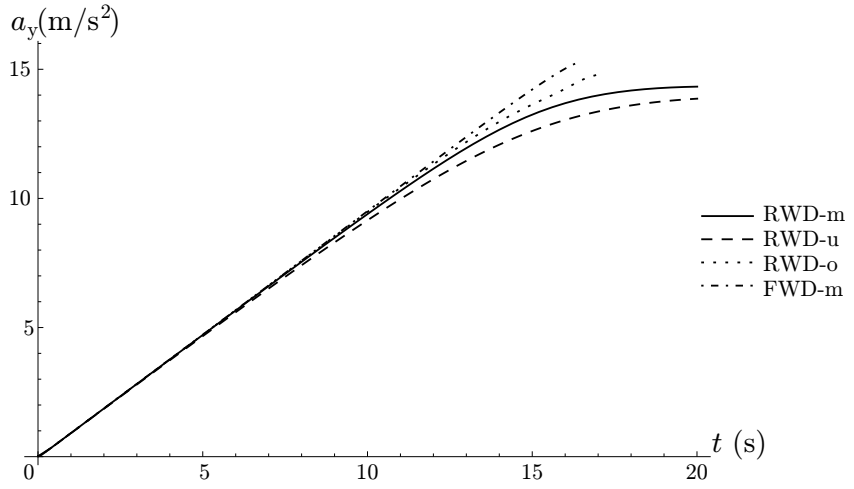

Figure 4. Lateral acceleration time history.

configurations reach higher lateral acceleration values in a shorter time, while RWD-u reaches the lowest lateral acceleration value.

A more effective representation of the vehicle handling is given in Fig. 5 where the classical handling diagram, as introduced in [1], is shown. The understeer coefficient was

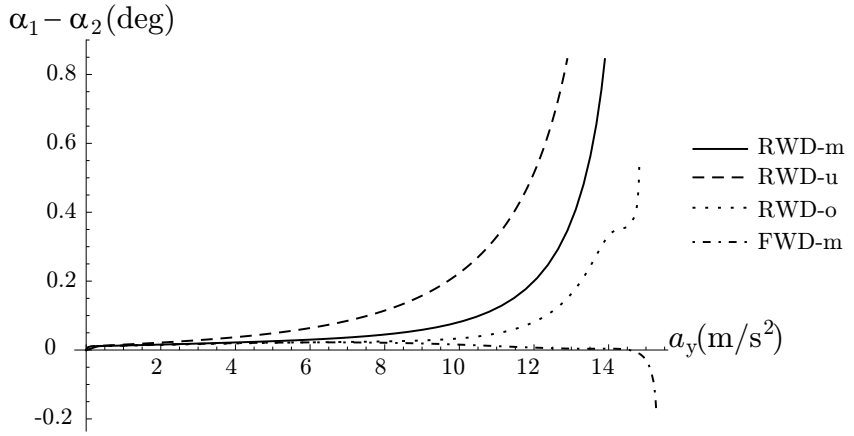

Figure 5. Handling diagram.

then computed differentiating the handling diagram profile with respect to the lateral acceleration

$$K = \frac{\partial(\alpha_1 - \alpha_2)}{\partial a_y} \tag{19}$$

and its profile is shown in Fig. 6. The RWD vehicle set-ups behaves as it could be predictable: the most understeering is the RWD-u while the least, among the RWD ones, is the RWD-o. This difference is due to the different axle load transfer for the two set-ups: the RWD-u set-up has more load transfer on the front axle and the front axle characteristic is worse [19] than the rear axle one. For this reason the understeer coefficient is higher along the whole acceleration range. The opposite happens for the RWD-o. The reference vehicle, RWD-m, has an halfway behavior.

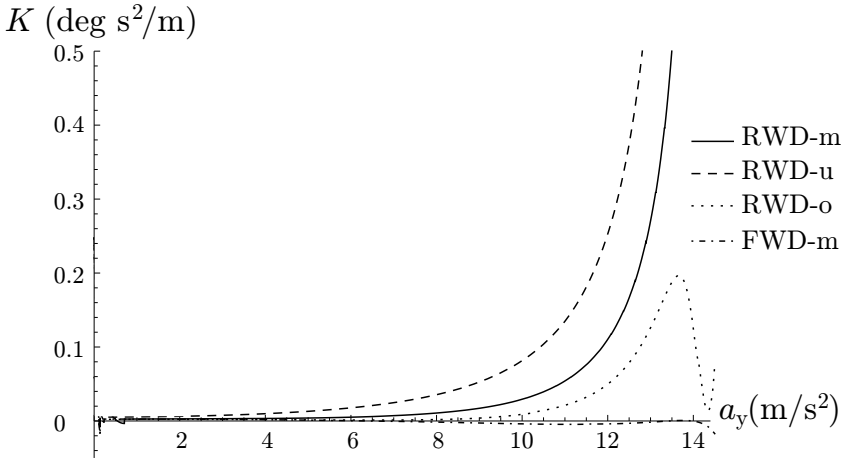

Figure 6. Understeer coefficient.

The understeer coefficient profile for the FWD-m is rather surprisingly: it is almost 0 in the whole lateral acceleration range, proving that, for the considered vehicle, this configuration is the least understeering among the ones considered. This is in contrast with what is usually found in the literature, but it is supported by the torque analysis proposed in the Section 7.

In addition to the classical way of computing the understeer coefficient, the new formula presented in Eq. 13 was used to compute K. It is worth noting that, for the considered maneuver, all the parameters, apart from $\dot{\rho}$, enclosed in Eq. 13 are constant. For this reason $\dot{\rho}$ was measured in the multibody model and its profile is shown in Fig. 7.

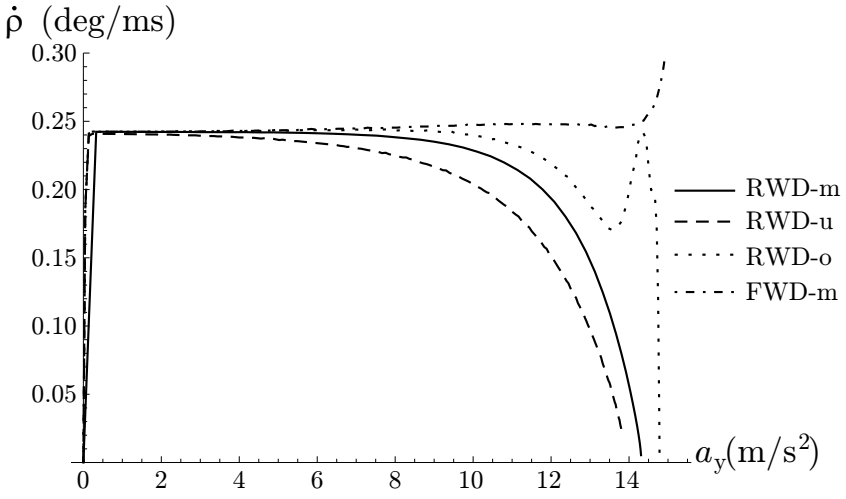

Figure 7. Time-derivative of the curvature ρ.

Figure 8 shows the comparison between the understeer coefficient computed following the classical formulation, which assumes the knowledge of the tire slip angles, and the new formulation, which assumes the knowledge of the sole curvature time-derivative $\dot{\rho}$. The differences between the two ways of computing the understeer parameter are almost null, and it is due to the quasi-steady state hypothesis (Eq. 10) and to the simplification made in Eq. 12 ($\ddot{\beta}u = 0$).

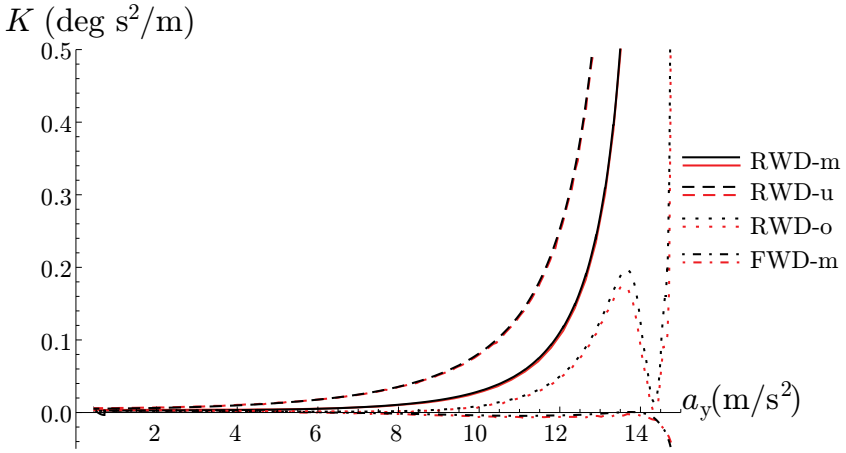

Figure 8. Comparison between the understeer coefficient computed considering the classical (black) and new (red) formulation.

It is worth noting that, in real vehicles, the measure of the tire slip angle is difficult to perform, while the curvature time derivative can be obtained with conventional gyros or accelerometers.

7. Yaw torque discussion

In this section the RWD-m and FWD-m simulations will be considered, in order to infer the influence of drive force on the vehicle handling behavior. Indeed, as stated in Eq. 5c, the drive forces affects both the yaw torque and the lateral dynamics. Section 4 distinguished three different contributions to the yaw torque: T_Y, T_f and T_d. T_Y is present in all the drive architectures, while the effect of T_f appears only if FWD or AWD are considered. Finally, T_d is present only in vehicle with non-open differential and this case is not discussed in this paper.

Figure 9 shows the yaw torque contributions for both RWD-m and FWD-m. The yaw torque due to the lateral force for RWD-m is almost constant up to 12 m/s^2 and then start decreasing due to the saturation of the front axle characteristic provoking understeer. Concerning FWD-m, the yaw torque due to lateral force start decreasing for lower values of lateral acceleration, since the front tire are undertaken in both longitudinal and lateral slip, but the torque T_f due to the drive force start increasing simultaneously. Indeed as the lateral acceleration rises, both the drive force and the steering wheel angle rises, provoking the increment of T_f.

The total yaw torque $\tilde{N}$ is shown in Fig. 10: concerning RWD-m its profile is identical to the T_y profile since $T_f = 0$, while for FWD-m it is almost constant within all the lateral acceleration range, provoking a less understeering behavior to the vehicle.

In order to furtherly support the results, the center of mass trajectory is shown in Fig. 11(a) where it is remarkable that the FWD-m vehicle drives a tighter trajectory under the same maneuver conditions. The path length of the FWD-m maneuver is shorter, since it is interrupted earlier as shown in Fig. 4, even if in correspondence of higher a lateral acceleration value. This is also confirmed by the steering wheel profile shown in Fig. 11 where, if the lateral acceleration is above 10 m/s^2, the steering wheel angle is lower for FWD-m than RWD-m

It is worth remarking that these results strongly depend on the combined characteristic

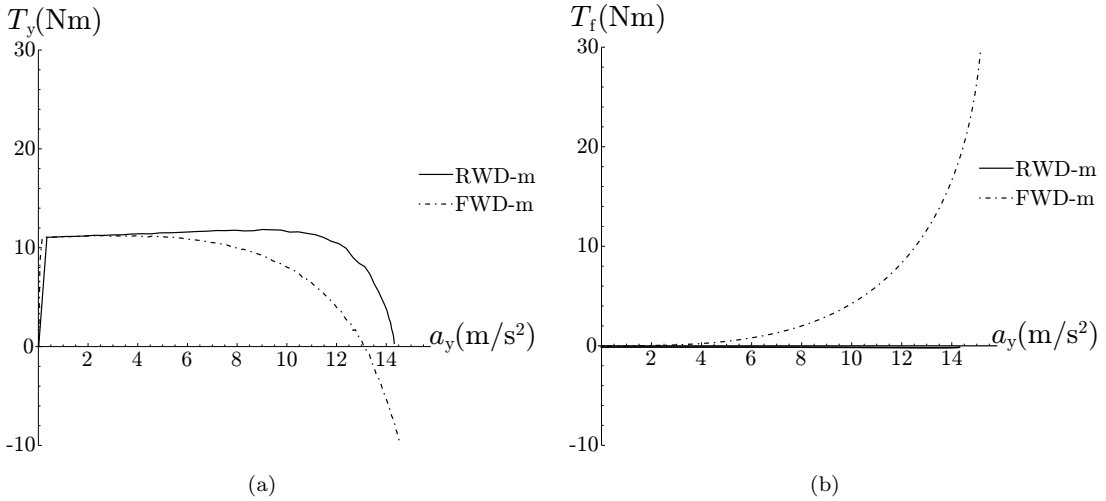

Figure 9. Yaw torque due to lateral (a) and drive forces(b) versus lateral acceleration.

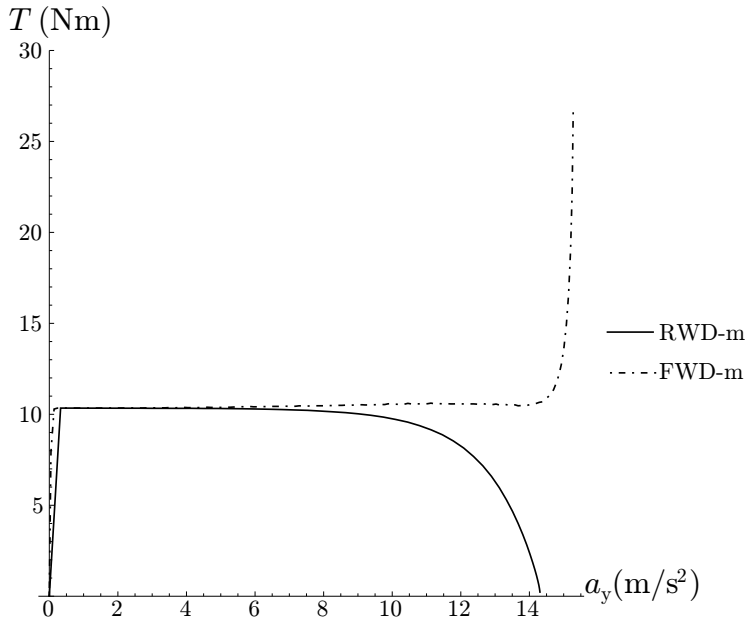

Figure 10. Yaw torque versus $\tilde{N}$ versus lateral acceleration.

of the tire model, since both the longitudinal and the lateral force have to be considered simultaneously.

8. Conclusions

In this paper a new formulation of the understeer coefficient was proposed. This is obtained in the case of constant speed maneuver and it is based on the knowledge of the steering wheel rate and the yaw rate time derivative. The main advantage of this formulation is that these quantities can be easily acquired in real vehicles with encoders, accelerometers or gyros which, in many cases, are already present in the vehicle. Indeed, considering the classical formulation, the tire slip angle are required which are difficult

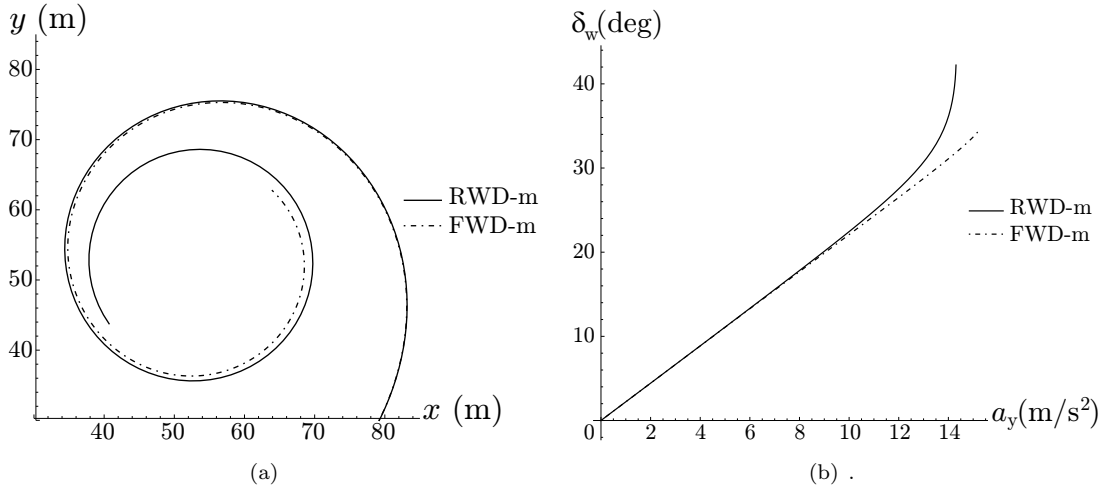

Figure 11. Center of mass trajectory (a) and steering wheel versus lateral acceleration (b).

to measure.

The effectiveness of the new formulation was proved with a multibody model, which was previously developed by the authors. In particular, the understeer coefficient computed following the classical method was compared to the one computed by the new method for different vehicle set-ups. No appreciable difference was found.

The new formulation allowed also to discuss about the relationship between the yaw torque and the understeer coefficient in an objective way. An alternative expression of the understeer coefficient, which is explicitly related to the vehicle yaw torque, was proposed. In the authors opinion, this formulation could be a base to develop yaw torque control which can keep the desired value of the understeer coefficient within the whole acceleration range.

Finally, basing on the yaw torque analysis, the influence of the drive architecture on the vehicle turning behavior was discussed. Apparently surprisingly it was found that, for the analyzed vehicle, the FWD architecture is less understeering than the RWD one. Indeed, even if the yaw torque due to the lateral forces in FWD decreases more quickly as the acceleration rises then in RWD, the yaw torque torque due to driving forces rises.

These results confirm the relationship between the understeer coefficient and the yaw torque presented in this paper, which can be used in yaw torque control to enhance vehicle performance and safety.

References

[1] Pacejka HB. Simplified analysis of steady-state turning behaviour of motor vehicles. Part 1. Handling diagrams of simple systems. Vehicle System Dynamics. 1973;2(3):161–172.

[2] Frendo F, Greco G, Guiggiani M, Sponziello A. The handling surface: a new perspective in vehicle dynamics. Vehicle System Dynamics. 2007;45(11):1001–1016.

[3] Frendo F, Greco G, Guiggiani M, Sponziello A. Evaluation of the vehicle handling performances by a new approach. Vehicle System Dynamics. 2008;46(S1):857–868.

[4] Frendo F, Greco G, Guiggiani M. Critical review of handling diagram and understeer gradient for vehicles with locked differential. Vehicle System Dynamics. 2006;44(6):431–447.

[5] Shibahata Y, Shimada K, Tomari T. Improvement of vehicle maneuverability by direct yaw moment control. Vehicle System Dynamics. 1993;22(5-6):465–481.

[6] Furukawa Y, Abe M. Advanced chassis control systems for vehicle handling and active safety. Vehicle System Dynamics. 1997;28(2-3):59–86.

[7] Van Zanten AT. Bosch ESP systems: 5 years of experience. SAE Technical Paper; 2000. Report.
[8] Shino M. Yaw-moment control of electric vehicle for improving handling and stability. JSAE Review. 2001;22(4):473–480.
[9] Osborn RP, Shim T. Independent control of all-wheel-drive torque distribution. Vehicle System Dynamics. 2006;44(7):529–546.
[10] Dugoff H, Fancher PS, Segel L. Tire performance characteristics affecting vehicle response to steering and braking contol inputs. Highway Safety Research Institute. 1969;.
[11] Piyabongkarn D, Lew JY, Rajamani R, Grogg JA, Yuan Q. On the use of torque-biasing systems for electronic stability control: limitations and possibilities. Control Systems Technology, IEEE Transactions on. 2007;15(3):581–589.
[12] Liang W, Yu H, McGee R, Kuang M, Medanic J. Vehicle pure yaw moment control using differential tire slip. In: American Control Conference. IEEE; 2009. p. 3331–3336.
[13] Wang J, Wang Q, Jin L, Song C. Independent wheel torque control of 4WD electric vehicle for differential drive assisted steering. Mechatronics. 2011;21(1):63–76.
[14] Ando N, Fujimoto H. Yaw-rate control for electric vehicle with active front/rear steering and driving/braking force distribution of rear wheels. In: Advanced Motion Control, 2010 11th IEEE International Workshop on. IEEE; 2010. p. 726–731.
[15] Mokhiamar O, Abe M. How the four wheels should share forces in an optimum cooperative chassis control. Control Engineering Practice. 2006;14(3):295–304.
[16] Ono E, Hattori Y, Muragishi Y, Koibuchi K. Vehicle dynamics integrated control for four-wheel-distributed steering and four-wheel-distributed traction/braking systems. Vehicle System Dynamics. 2006;44(2):139–151.
[17] Bartolozzi R, Bucchi F, Frendo F. A multibody model of a formula student car. On-track validation and set-up optimization. 2nd International Multibody System Dynamics (IMSD) Conference - Stuttgart, Germany. 2012;.
[18] Kuiper E, Van Oosten JJM. The PAC2002 advanced handling tire model. Vehicle System Dynamics. 2007;45(S1):153–167.
[19] Guiggiani M. The science of vehicle dynamics - Handling, braking, and ride of road and race cars. Springer; 2014.